

primary magnetic response of single-crystal Fe whiskers are accurately characterized by a model for localized magnons on a Gaussian size distribution of independently relaxing domains.

REFERENCES AND NOTES

1. T. H. O'Dell, *Ferromagnetodynamics* (Wiley, New York, 1981).
2. R. H. Victora, *Phys. Rev. Lett.* **58**, 1788 (1987).
3. D. D. Awschalom, D. P. DiVincenzo, J. F. Smyth, *Science* **258**, 414 (1992).
4. A. D. Berk, *J. Appl. Phys.* **28**, 190 (1957).
5. D. S. Rodbell, *ibid.* **30**, 187S (1959).
6. R. V. Chamberlin, R. Böhmer, E. Sanchez, C. A. Angell, *Phys. Rev. B* **46**, 5787 (1992).
7. R. V. Chamberlin and M. R. Scheinfein, *Ultramicroscopy* **47**, 408 (1992).
8. C. Kittel and J. K. Galt, *Solid State Phys.* **3**, 437 (1956).
9. B. D. Cullity, *Introduction to Magnetic Materials* (Addison-Wesley, Menlo Park, CA, 1972), chap. 12.
10. L. Néel, *Ann. Geophys.* **5**, 99 (1949); *Adv. Phys.* **4**, 191 (1955).
11. A. P. Malozemoff and E. Pytte, *Phys. Rev. B* **34**, 6579 (1986).
12. D. S. Fisher and D. A. Huse, *Phys. Rev. Lett.* **56**, 1601 (1986).
13. E. C. Stoner and E. P. Wohlfarth, *Philos. Trans. R. Soc. London* **240**, 599 (1948).
14. R. H. Victora, *Phys. Rev. Lett.* **63**, 457 (1989).
15. R. V. Chamberlin and D. N. Haines, *ibid.* **65**, 2197 (1990).
16. ———, D. W. Kingsbury, *J. Non-Cryst. Solids* **131–133**, 192 (1991).
17. R. V. Chamberlin and F. Holtzberg, *Phys. Rev. Lett.* **67**, 1606 (1991).
18. S. S. Brenner, *Acta Metall.* **4**, 62 (1956).
19. C. Kittel, *Phys. Rev.* **70**, 965 (1946).
20. R. W. de Blois and C. D. Graham, Jr., *J. Appl. Phys.* **29**, 931 (1958).
21. H. J. Williams, W. Shockley, C. Kittel, *Phys. Rev.* **80**, 1090 (1950).
22. R. V. Coleman and G. F. Scott, *ibid.* **107**, 1276 (1957).
23. F. Mezei, *J. Magn. Magn. Mater.* **31–34**, 1327 (1983).
24. ———, *Phys. Rev. Lett.* **49**, 1096 (1982).
25. H. G. Bohn, A. Kollmar, W. Zinn, *Phys. Rev. B* **30**, 6504 (1984).
26. K. Schmidt-Rohr and H. W. Spiess, *Phys. Rev. Lett.* **66**, 3020 (1991).
27. M. E. Schabes and H. N. Bertram, *J. Appl. Phys.* **64**, 1347 (1988).
28. P. Choquard and J. Clerouin, *Phys. Rev. Lett.* **50**, 2086 (1983).
29. R. Kupo, *J. Phys. Soc. Jpn.* **17**, 975 (1962).
30. The H solenoid had a time constant of $\sim 3 \times 10^{-6}$ s, after which μ -metal and superconducting shields reduced the residual field to $H_0 \approx 0.8$ mOe. Net magnetization in the (100)-direction was measured by concentric, second-order gradiometer, flux-transformer coils connected to the SQUID. Absolute magnetization was determined before and after each relaxation by movement of the sample between two of the counterwound coils.
31. C. Heiden and H. Rogalla, *J. Magn. Magn. Mater.* **19**, 240 (1980).
32. In Fig. 3A, for $H > 10$ Oe, M/H approaches saturation, $M_s = 223$ emu g^{-1} . For $H < 10$ Oe, the demagnetization factor ($N/4\pi = 0.00144$ for an aspect ratio of 50:1) limits the net magnetization to $M/H = 1/N \approx 55$ emu $cm^{-3} \approx 5.6$ emu g^{-1} . Thus, below saturation, demagnetization reduces the net internal field by a factor $H_i/H \approx 0.3$, which is estimated from the ratio of measured to known magnetization at saturation $M(H_s)/M_s \approx (6.5 \times 10)/223 \approx 0.3$, consistent with the ratio of known to apparent saturation fields $H_s/10 \approx 0.3$.
33. T. Holstein and H. Primakoff, *Phys. Rev.* **58**, 1098 (1940).
34. R. Pauthenet, *J. Appl. Phys.* **53**, 2029 (1982).
35. B. Heinrich and A. S. Arrott, *Can. J. Phys.* **50**, 710 (1972).
36. Eddy currents could influence the net relaxation rate, but our observation of no change between 4 and 40 K indicates that the temperature-dependent resistivity [G. R. Taylor, A. Isin, R. V. Coleman, *Phys. Rev.* **165**, 621 (1969)] does not play a role.
37. We thank A. S. Arrott for supplying the Fe whiskers, which were grown at Simon Fraser University (Burnaby, British Columbia) under an operating grant from the Natural Sciences and Engineering Research Council of Canada. We have benefited from conversations with M. A. Glaser, O. F. Sankey, K. E. Schmidt, and R. H. Victora. This research was supported by Office of Naval Research contract N00014-88-K-0094.

kers, which were grown at Simon Fraser University (Burnaby, British Columbia) under an operating grant from the Natural Sciences and Engineering Research Council of Canada. We have benefited from conversations with M. A. Glaser, O. F. Sankey, K. E. Schmidt, and R. H. Victora. This research was supported by Office of Naval Research contract N00014-88-K-0094.

1 December 1992; accepted 9 March 1993

South Asian Summer Monsoon Variability in a Model with Doubled Atmospheric Carbon Dioxide Concentration

Gerald A. Meehl* and Warren M. Washington

Doubled atmospheric carbon dioxide concentration in a global coupled ocean-atmosphere climate model produced increased surface temperatures and evaporation and greater mean precipitation in the south Asian summer monsoon region. As a partial consequence, interannual variability of area-averaged monsoon rainfall was enhanced. Consistent with the climate sensitivity results from the model, observations showed a trend of increased interannual variability of Indian monsoon precipitation associated with warmer land and ocean temperatures in the monsoon region.

Variability of the south Asian summer monsoon, of which the Indian monsoon is a major part, is manifested by extreme events (droughts and floods) that have considerable impacts on human society and agriculture. Previous climate-modeling studies have shown greater mean south Asian summer monsoon rainfall attributable to climate change caused by an increase of atmospheric CO_2 concentration (1). However, changes in variability that probably are of greater importance to society (2) have received little attention (3). This is so because global coupled ocean-atmosphere climate models capable of internally generating some aspects of variability of the coupled climate system have only recently been integrated for a sufficient length of time to begin to address such issues. In this report, we describe possible changes to south Asian summer monsoon variability based on a global coupled ocean-atmosphere climate model and compare the results with observations. This comparison allowed us to identify physical processes that may contribute to changes in south Asian monsoon variability in a future CO_2 -enriched climate.

In our simulation, the global atmospheric model had an approximate horizontal resolution of 4.5° latitude by 7.5° longitude and nine vertical levels. Clouds were computed, and soil moisture was parameterized by a simple reservoir formulation. The global ocean model had a coarse grid (5° by 5°)

and four vertical layers and included a simple thermodynamic formulation for the freezing and melting of sea ice. Coupling between the model components involved sea-surface temperature (SST) from the ocean and net heat flux, freshwater flux, and wind stress from the atmosphere.

The global coupled ocean-atmosphere climate model contains errors that are the products of flaws in each of the components as well as errors compounded by coupled interactions at the air-sea interface (4). The errors in the basic state are representative of the inherent limitations of the current generation of coupled models and reflect our lack of understanding of certain coupled processes in the observed climate system and our inability to fully capture such processes in models. Yet, this model and others like it have been shown to simulate successfully fundamental features of the coupled climate system. Consequently, they have been quite useful for basic CO_2 climate sensitivity studies, for insight into coupled processes in the observed system, and for preliminary indications to policy-makers of possible future climate changes (1, 3). Previous results for CO_2 climate sensitivity (3) and process studies (5) are similar in various models in spite of different formulations, types of model errors, and degrees of model error correction. This similarity suggests that there is a robustness of the climate simulations that gives us a degree of confidence in the results.

Because there are no corrections that force the model climate to the observed

National Center for Atmospheric Research, Boulder, CO 80307–3000.

*To whom correspondence should be addressed.

state, the coupled ocean-atmosphere model produces tropical SSTs that are cooler and more zonally uniform than observed (1, 3, 6–8). Consequently, the overall land-sea temperature contrast, the fundamental forcing of the monsoon circulation (9), is enhanced in the coupled model compared with the observed system. This enhancement contributes to greater onshore flow, less rainfall over ocean, and somewhat more rainfall over land, particularly over Bangladesh, compared with observations and a simulation with the same model that had SSTs prescribed to observed values (6, 10). Even with this systematic error in the coupled model, the basic monsoon seasonal evolution and rainfall patterns are still comparable with observations.

We focused on results from years 21 to 65 (time series from the model are available after year 20) of the control run with present atmospheric CO₂ concentration (1 × CO₂) compared with an experiment with doubled CO₂ concentration (2 × CO₂). The doubled CO₂ experiment had larger climate anomalies (greater signal-to-noise ratio) than a transient experiment over the same period in which CO₂ increased 1% per year (6). The overall features at the end of the transient integration were similar to those throughout the 2 × CO₂ experiment. Therefore, the conclusions derived from the 2 × CO₂ experiment are likely to be robust with respect to the history of CO₂ input. Results for the Indian area were similar to those from the larger south Asian region in the model, and thus we make qualitative comparisons between the model results and an index of area-averaged precipitation covering only India (11). Model results are for the seasonal average of June, July, and August, whereas the observed index is for June through September (model results are similar for June through September).

For both the control case (Fig. 1A) and the case with doubled CO₂ concentration (Fig. 1B), the south Asian monsoon precipitation averaged for all land points in the area 5° to 40°N, 60° to 100°E showed little trend over the 45-year period. Though not at final equilibrium, this is consistent with the small trends of globally averaged temperature on this time scale in the model (8). The mean south Asian precipitation in the control case (6.40 mm day⁻¹) was somewhat less than the 45-year (1946 to 1990) observed Indian monsoon index (6.99 mm day⁻¹). The standard deviation (SD) of area-averaged precipitation from the control case (0.49 mm day⁻¹) was also less than observed (0.71 mm day⁻¹). If precipitation from only the nine grid points over India were averaged from the model, the mean of 7.01 mm day⁻¹ was close to the observed value, but the SD was higher (1.40 mm day⁻¹). The control simulation

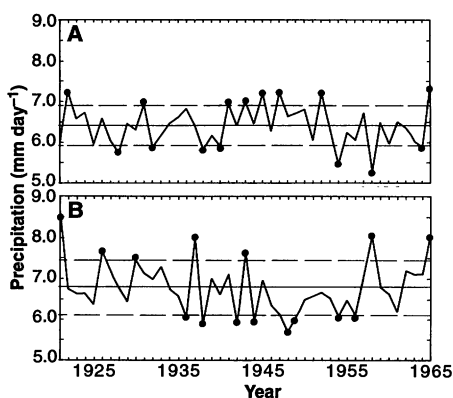


Fig. 1. Area-averaged summer (June through August) monsoon precipitation in south Asia (5° to 40°N, 60° to 100°E) in millimeters per day for (A) the control case (present CO₂ concentration) and (B) the case of doubled CO₂ concentration. Solid line is the 45-year mean; dashed lines indicate 1 SD; dots indicate the years used in the weak and strong monsoon composites.

appears to have generated about the right range of interannual variability for this 45-year period compared with the observed monsoon, although the variability over India itself was somewhat larger.

For the simulation with doubled CO₂ concentration, the area-averaged mean south Asian precipitation increased by 6.3% to 6.80 mm day⁻¹ with an SD of 0.65 mm day⁻¹. Consistent with other models (1), this increase in mean precipitation can be attributed to land areas warming faster than oceans. Thus, the land-sea temperature contrast was enhanced, and moisture convergence over land intensified. In addition, the variability of monsoon precipitation was greater than that in the control case (SD increased to 0.65 mm day⁻¹ from 0.49 mm day⁻¹; an F test on the variances showed the increased variability significant at the 5% level).

To examine changes in the absolute amounts of precipitation, we defined weak and strong monsoon seasons when area-averaged precipitation was more than 1 SD from the mean (Fig. 1). The mean precipitation in the weak monsoon years was only slightly higher for the 2 × CO₂ case (5.97 mm day⁻¹) than for the control (5.69 mm day⁻¹). However, the average precipitation in strong years was considerably greater in the 2 × CO₂ experiment (7.95 versus 7.14 mm day⁻¹). This increase was a result of both the higher mean precipitation and enhanced variability in the simulation with doubled CO₂ concentration.

The geographical distribution of the differences, important for determination of what areas are most affected by monsoon variability in the model, showed that the precipitation difference pattern of weak minus strong years was similar in both the control and the 2 × CO₂ cases (Fig. 2).

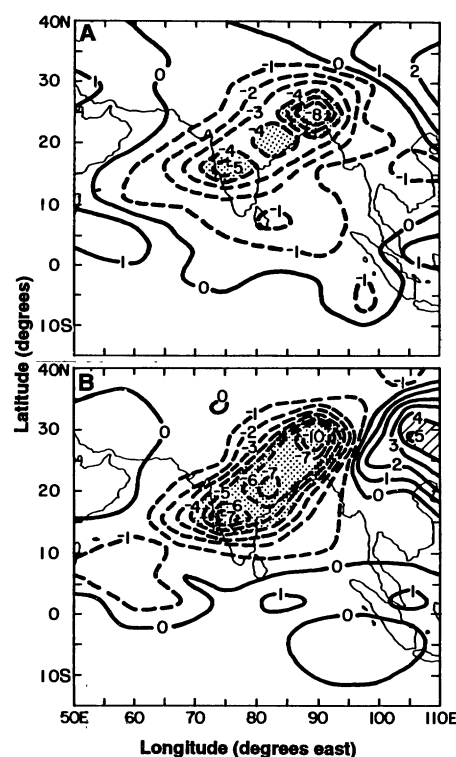


Fig. 2. Weak minus strong monsoon composite differences (millimeters per day), June through August. (A) 1 × CO₂ control case, (B) 2 × CO₂ case. Differences greater than 4.0 mm day⁻¹ are stippled (negative) or hatched (positive).

Moisture deficits in weak years covered most of India and Bangladesh with increases above the mean in east Asia. This pattern has also been seen in observed rainfall variability over southern Asia (12). However, the magnitude of the differences was greater in the simulation with doubled CO₂ concentration (about 2 mm day⁻¹), indicative of the enhanced variability noted for area-averaged precipitation (Fig. 1).

Area-averaged differences of other elements involved with the hydrological cycle for the 1 × CO₂ case (Table 1) showed a warmer, drier land surface with less evaporation and decreased precipitation and evaporation over ocean areas, which is representative of weak monsoon conditions. Consistent with observations (13, 14), there was less moisture flux from the Indian Ocean as well as a reduced land-surface moisture supply during weak monsoons in the coupled model.

In the doubled CO₂ case (Table 1), the sign of the differences was the same as in the control case (except for Indian Ocean SST, for which the area-averaged differences were near zero in both cases), but the magnitudes were greater. Thus, there was enhanced variability in other hydrological elements in addition to precipitation. A major process that contributed to this increased variability was a consequence of higher mean surface temperatures (caused

Table 1. Area averages computed over south Asia (land points in the area 5° to 40°N, 60° to 100°E) and the Indian Ocean (ocean points in the area 15°S to 30°N, 40° to 110°E). Weak and strong monsoon years for the control ($1 \times \text{CO}_2$) case and the $2 \times \text{CO}_2$ case are taken from Fig. 1 for area-averaged south Asian precipitation that exceeds 1 SD.

| Elements of hydrological cycle | $1 \times \text{CO}_2$ | | | $2 \times \text{CO}_2$ | | |
|--|------------------------|--------|--------------|------------------------|--------|--------------|
| | Weak | Strong | Difference | Weak | Strong | Difference |
| <i>South Asia</i> | | | | | | |
| Surface temperature (K) | 299.83 | 299.07 | +0.76 | 301.28 | 300.16 | +1.12 |
| Precipitation (mm day^{-1}) | 5.69 | 7.14 | -1.45 (-25%) | 5.97 | 7.95 | -1.98 (-33%) |
| Evaporation (mm day^{-1}) | 3.07 | 3.67 | -0.60 (-20%) | 3.21 | 3.97 | -0.76 (-24%) |
| Soil moisture (cm) | 3.86 | 4.76 | -0.90 (-23%) | 3.79 | 5.19 | -1.40 (-37%) |
| <i>Indian Ocean</i> | | | | | | |
| Surface temperature (K) | 297.25 | 297.32 | -0.07 | 298.32 | 298.30 | +0.02 |
| Precipitation (mm day^{-1}) | 4.12 | 4.46 | -0.34 (-8%) | 4.32 | 4.70 | -0.38 (-9%) |
| Evaporation (mm day^{-1}) | 4.61 | 4.75 | -0.14 (-3%) | 4.76 | 4.95 | -0.19 (-4%) |

in this case by the increase of CO_2 concentration) that produced a nonlinear increase of evaporation (15) and proportionately greater mean moisture sources in the $2 \times \text{CO}_2$ case (note the larger negative differences for the $2 \times \text{CO}_2$ case for precipitation, evaporation, and soil moisture over south Asia and precipitation and evaporation over the Indian Ocean).

Another major influence on variability in the Asian monsoon is El Niño–Southern Oscillation (ENSO). Phenomena similar to ENSO occur in the coupled model (SST anomalies develop in the eastern Pacific and subsequently become established in the central equatorial Pacific), and the influence of ENSO is felt in the Asian monsoon sector as observed (16). For example, the correlation between area-averaged sea-level pressure (an indicator of monsoon strength) for the June through August season over the Indian Ocean and SST in the eastern tropical Pacific (10°S to 10°N, 150° to 90°W, referred to as Niño3) was +0.54 during a 50-year period in the coupled model (years 21 to 70 in the control run; high pressure indicative of a weak monsoon was positively correlated with high SSTs in the tropical Pacific). In terms of ENSO event phenomena, 5 of the 8 years with extreme anomalously warm SSTs in the Niño3 area were associated with below normal south Asian monsoons; 6 of 9 years with extreme anomalously cold SSTs in the Niño3 area had above normal monsoons. Therefore, there was a link between SST anomalies associated with ENSO-like phenomena in the tropical Pacific and the strength of the south Asian monsoon in the coupled model, but this connection was weaker than that observed (17). Another regional process associated with monsoon variability in the model was Asian snow cover in the spring before the summer monsoon season. As observed (14, 18, 19), increased snow cover in the model was associated with weak monsoons and warm SSTs in the tropical Pacific and vice versa for decreased

snow cover in both the control and doubled CO_2 cases.

These results, along with those presented in a study of changes to ENSO-like phenomena in the coupled model with doubled CO_2 concentration (7), showed that there would be some enhanced contribution to a weaker monsoon during years with anomalously warm SSTs in the tropical Pacific with doubled CO_2 and vice versa for cool SSTs. These influences from ENSO-like phenomena in the doubled CO_2 climate would add to the regional processes described above to produce enhanced variability of monsoon precipitation.

For a comparison with the model results, we examined observed surface-air temperature anomalies (1, 3, 20, 21) and the Indian monsoon index for two 20-year periods from the post-World War II era (Fig. 3). These data showed that both the south Asian monsoon land area and the Indian Ocean warmed more from 1971 to 1990 than from 1946 to 1965 but that the warming was greater over the Indian Ocean (an absolute increase of 0.28°C compared with 0.07°C over land). Consistent with this decrease in land-sea temperature contrast, monsoon rainfall over India was less from 1971 to 1990 (6.87 mm day^{-1}) than from 1946 to 1965 (7.17 mm day^{-1}). Calculations made from separate 5-year periods were similar. Various models (including the present one) have been shown to reproduce this basic relation (decreased land-sea temperature contrast associated with a weak monsoon and vice versa for a strong monsoon) for various boundary forcing conditions (22). Yet, in the model with doubled CO_2 concentration, although both land and ocean warmed, the land warmed faster than the ocean, thus increasing the mean land-sea temperature difference; this difference intensified the mean monsoon in contrast to the trend in the observations. However, the observations are consistent with the model results concerning variability in that the SD of monsoon precipitation over

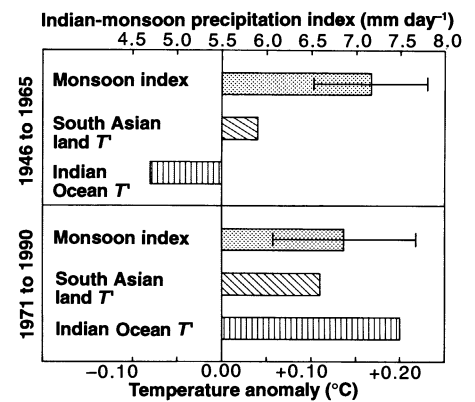


Fig. 3. Twenty-year averages for 1946 to 1965 and 1971 to 1990 for an all-India monsoon precipitation index (top axis), June through September (11), and annual mean area averages computed over south Asia (land points only in the area 5° to 40°N, 60° to 100°E) and the Indian Ocean (ocean points only in the area 15°S to 30°N, 40° to 110°E) for observed surface air temperature anomalies T' (bottom axis) relative to the 1951 to 1980 mean (1, 3, 20, 21).

India during 1971 to 1990 increased to 0.79 mm day^{-1} (from 0.64 mm day^{-1} during 1946 to 1965) as both land and ocean surface temperatures rose. Also consistent with the model results are observed increases of evaporation that have been documented for the tropical oceans in the more recent period (23, 24).

This model (and others) is able to reproduce many elements of the monsoon associated with land-sea temperature contrast (14, 18, 19, 22) and is also capable of representing most known coupled processes that affect monsoon interannual variability. Consequently, it is likely that the model is at least qualitatively correct in its representation of increased interannual monsoon variability, which agrees with observations. The discrepancy with observed changes of recent land-sea temperature difference and mean monsoon strength implies that there is low-frequency variability in the observed system in addition to the forcing from increased CO_2 . Resolution of these issues requires an increased understanding of the processes that determine decadal and longer time scale changes of SST, land temperatures, and precipitation in the observed monsoon system (11, 25) and improved global coupled climate models, especially in regards to land-surface processes.

REFERENCES AND NOTES

1. J. T. Houghton, G. J. Jenkins, J. J. Ephraums, Eds., *Climate Change: The IPCC Scientific Assessment* (Cambridge Univ. Press, Cambridge, 1990).
2. R. W. Katz and B. G. Brown, *Clim. Change* 21, 289 (1992).
3. J. T. Houghton, B. A. Callander, S. K. Varney, Eds., *Climate Change 1992: The IPCC Scientific Assembly Supplementary Report* (Cambridge

- Univ. Press, Cambridge, 1992).
4. G. A. Meehl, in *Climate Systems Modeling*, K. Trenberth, Ed. (Cambridge Univ. Press, Cambridge, 1992), p. 555.
 5. *WCRP-68, WMO/TD No. 470*, (World Meteorological Organization, Geneva, 1992).
 6. W. M. Washington and G. A. Meehl, *Clim. Dyn.* **4**, 1 (1989).
 7. G. A. Meehl, G. W. Branstator, W. M. Washington, *J. Clim.* **6**, 42 (1993).
 8. G. A. Meehl, W. M. Washington, T. R. Karl, *Clim. Dyn.* **8**, 117 (1993).
 9. P. J. Webster, in *Monsoons*, J. S. Fein and P. L. Stephens, Eds. (Wiley, New York, 1987), pp. 3–32.
 10. G. A. Meehl, *J. Clim.* **2**, 1146 (1989).
 11. B. Parthasarathy, K. Rupa Kumar, A. A. Munot, *ibid.* **4**, 927 (1991).
 12. K.-M. Lau and P. J. Sheu, in *Teleconnections Linking Worldwide Climate Anomalies*, M. H. Glantz, R. W. Katz, N. Nicholls, Eds. (Cambridge Univ. Press, Cambridge, 1991), pp. 227–256.
 13. A. Kitoh, *J. Meteorol. Soc. Jpn.* **70**, 563 (1992).
 14. T. Yasunari, A. Kitoh, T. Tokioka, *ibid.* **69**, 473 (1991).
 15. G. L. Stephens, *J. Clim.* **3**, 634 (1990).
 16. G. A. Meehl, *ibid.*, p. 72.
 17. E. M. Rasmusson and T. H. Carpenter, *Mon. Weather Rev.* **111**, 517 (1983).
 18. J. Shukla, in (9), pp. 399–464.
 19. T. P. Barnett, L. Dumenil, U. Schlese, E. Roeckner, M. Latif, *J. Atmos. Sci.* **46**, 661 (1989).
 20. P. D. Jones, *J. Clim.* **1**, 654 (1988).
 21. M. Bottomley, C. K. Folland, J. Hsiung, R. E. Newell, D. E. Parker, *Global Ocean-Surface Temperature Atlas* (U.K. Meteorological Office, Bracknell, U.K., 1990).
 22. G. A. Meehl, "Simulation of Interannual and Intraseasonal Monsoon Variability," in *WCRP-68, WMO/TD No. 470* (World Meteorological Organization, Geneva, 1991), pp. 2.101–2.107.
 23. H. Flohn, A. Kapala, H. R. Knoche, H. Machel, *Clim. Dyn.* **4**, 237 (1990).
 24. D. J. Gaffen, T. P. Barnett, W. P. Elliott, *J. Clim.* **4**, 989 (1991).
 25. J. Shukla, in *Climate Change: Science, Impacts, and Policy*, J. Jager and H. L. Ferguson, Eds. (Cambridge Univ. Press, Cambridge, 1991), pp. 203–210.
 26. A portion of this study is supported by the Office of Health and Environmental Research, U.S. Department of Energy, as part of its Carbon Dioxide Research Program. The National Center for Atmospheric Research is sponsored by the National Science Foundation.

6 November 1992; accepted 4 March 1993

A 3620-Year Temperature Record from *Fitzroya cupressoides* Tree Rings in Southern South America

Antonio Lara* and Ricardo Villalba

A tree-ring width chronology of alerce trees (*Fitzroya cupressoides*) from southern Chile was used to produce an annually resolved 3622-year reconstruction of departures from mean summer temperatures (December to March) for southern South America. The longest interval with above-average temperatures was from 80 B.C. to A.D. 160. Long intervals with below-average temperatures were recorded from A.D. 300 to 470 and from A.D. 1490 to 1700. Neither this proxy temperature record nor instrumental data for southern South America for latitudes between 35° and 44°S provide evidence of a warming trend during the last decades of this century that could be related to anthropogenic causes. The data also indicate that alerce is the second longest living tree after the bristlecone pine (*Pinus longaeva*).

Climatic records from weather stations as well as proxy sources are scant for the Southern Hemisphere compared with those for the Northern Hemisphere (1–4). However, Southern Hemisphere climate records are crucial for understanding the global climatic system because climatic differences between the Northern and Southern hemispheres could provide relevant clues to the mechanisms that underlie global climatic change (5). Long, high-resolution paleotemperature records from the Southern Hemisphere are needed to assess the spatial patterns and extent of global warming (2). Here, we present an annually resolved, 3622-year summer temperature reconstruction from a tree-ring width chronology of

alerce trees (*Fitzroya cupressoides*) from southern Chile.

Southern South America presents a unique opportunity for obtaining terrestrial climate proxy records in a region that is under the influence of both Antarctic and mid-latitude atmospheric circulation patterns (6). Tree-ring records from Argentina and Chile have proved useful for temperature and precipitation reconstruction (7, 8) as well as for estimating the latitudinal shifts of the Pacific high-pressure cell (9) and the occurrence of El Niño–Southern Oscillation events (10). Earlier studies of alerce produced a 1534-year ring-width chronology (11) and a 1120-year reconstruction of mean summer temperature variations for northern Patagonia (7).

We collected radial wedges from alerce stumps from a mixed conifer–broad-leaved stand that was logged from 1975 to 1976 and cores from living trees taken with increment borers in other nearby unlogged

stands. These stands were located at 860- to 890-m elevation on the western slope of the Andes near Lenca in south-central Chile (41°33'S, 72°36'W; Fig. 1). The climate at the site is oceanic temperate with decreases in the summer rainfall (12). Lago Chapo, 18 km northeast of the study site at 240-m elevation, has a mean annual temperature of 10.3°C and receives 4140 mm of mean annual precipitation (13). Radial wedges and cores were surfaced and cross-dated, and ring widths were measured according to standard methods (14).

Of the 96 samples examined, only 43 radii (21 wedges and 22 cores) from 38 trees were successfully cross-dated. The mean length radii was 867 years (the range was 325 to 2248 years). The oldest alerce tree was dated from a wedge collected from a stump of a tree cut in 1975. Cross dating of the inner 1440 years of this tree indicated that it was 3613 years old. There were 57 locally absent rings out of a total of 37,260 rings in the cross-dated data set (0.15%). We detrended ring widths into dimensionless indices to remove the effects of changes in tree growth that resulted from aging, to homogenize the mean and variance, and to produce a standard chronology for the site (15). Different curve-fitting procedures for the computation of the tree-ring indices were tested (16). Pre-whitened residual series were combined to produce a mean chronology suitable for climate reconstruction.

Paleoclimatic interpretation of the Lenca chronology was based on the relation between alerce growth (expressed as annual tree-ring indices) and available regional temperature and precipitation records from Chile and Argentina between 39° and 44°S. We investigated these relations using response and correlation functions (17, 18) for various monthly and seasonal combinations of the meteorological records. There was a significant negative linear relation (slope = -2.24 ; SE = 0.45) between alerce tree-ring indices and previous summer (December to March) mean temperature for the period from 1910 to 1987 for a regional average of the following meteorologic stations: Colluncó, Bariloche, Esquel, Mascaradi, and Sarmiento. These stations are located in Argentina east of the Andes, 140 to 485 km from the study site (Fig. 1). A similar but weaker negative relation between tree-ring indices and mean prior summer temperature (slope = -1.57 ; SE = 0.54) was seen for the interval from 1910 to 1987 with the use of a regional record from four stations (Valdivia, Isla Teja, Punta Galera, and Lago Chapo) located in Chile west of the Andes, 18 to 170 km from the sampling site (Fig. 1). The larger standard error associated with this regional record may be because the Chilean stations are

A. Lara, Laboratory of Tree-Ring Research, University of Arizona, Tucson, AZ 80721.
R. Villalba, Department of Geography, University of Colorado, Boulder, CO 80309.

*Present address: Instituto de Silvicultura, Universidad Austral de Chile, Casilla 567, Valdivia, Chile.